Atmos. Chem. Phys., 11, 7143–7153, 2011
www.atmos-chem-phys.net/11/7143/2011/
doi:10.5194/acp-11-7143-2011

Atmospheric Chemistry and Physics

Coupled vs. decoupled boundary layers in VOCALS-REx

C. R. Jones[1], **C. S. Bretherton**[2], **and D. Leon**[3]

[1]Department of Applied Mathematics, University of Washington, Seattle, Washington, USA
[2]Department of Atmospheric Sciences, University of Washington, Seattle, Washington, USA
[3]Department of Atmospheric Science, University of Wyoming, Laramie, Wyoming, USA

Received: 3 March 2011 – Published in Atmos. Chem. Phys. Discuss.: 11 March 2011
Revised: 15 July 2011 – Accepted: 15 July 2011 – Published: 21 July 2011

Abstract. We analyze the extent of subtropical stratocumulus-capped boundary layer decoupling and its relation to other boundary-layer characteristics and forcings using aircraft observations from VOCALS-REx along a swath of the subtropical southeast Pacific Ocean running west 1600 km from the coast of Northern Chile. We develop two complementary and consistent measures of decoupling. The first is based on boundary layer moisture and temperature stratification in flight profiles from near the surface to above the capping inversion, and the second is based the difference between the lifted condensation level (LCL) and a mean lidar-derived cloud base measured on flight legs at 150 m altitude. Most flights took place during early-mid morning, well before the peak in insolation-induced decoupling.

We find that the boundary layer is typically shallower, drier, and well mixed near the shore, and tends to deepen, decouple, and produce more drizzle further offshore to the west. Decoupling is strongly correlated to the "mixed layer cloud thickness", defined as the difference between the capping inversion height and the LCL; other factors such as wind speed, cloud droplet concentration, and inversion thermodynamic jumps have little additional explanatory power. The results are broadly consistent with the deepening-warming theory of decoupling.

In the deeper boundary layers observed well offshore, there was frequently nearly 100 % boundary-layer cloud cover despite pronounced decoupling. The cloud cover was more strongly correlated to a κ parameter related to the inversion jumps of humidity and temperature, though the exact functional relation is slightly different than found in prior large-eddy simulation studies.

Correspondence to: C. R. Jones
(cjones@amath.washington.edu)

1 Introduction

The simplest realistic model of subtropical stratocumulus consists of a single, well-mixed boundary layer in which vigorous turbulence stirs the moist-conserved variables liquid potential temperature θ_ℓ, approximated as

$$\theta_\ell \approx \theta - \frac{L}{c_p} q_\ell, \tag{1}$$

and total water mixing ratio

$$q_T = q_\ell + q_v \tag{2}$$

into vertically uniform profiles below a capping temperature inversion at height z_i. Here, θ is the potential temperature, L is the latent heat of vaporization for water, c_p is the specific heat of dry air at constant pressure, q_ℓ is the liquid water mixing ratio and q_v is the water vapor mixing ratio. Mixed-layer models (MLMs) (e.g. Lilly, 1968), which prognose the evolution of the boundary-layer θ_ℓ, q_T and z_i assuming this well-mixed structure, have provided many insights into the structure and maintenance of subtropical stratocumulus layers.

In contrast, decoupling of the boundary layer occurs when the turbulence does not maintain a well-mixed layer. The radiatively driven turbulence in the cloud layer becomes separated from that of the surface-flux driven subcloud layer, and the two layers become "decoupled" in the sense that each layer itself is well-mixed, but mixing between the cloud and subcloud layer is inhibited by the presence of a stable layer between them (Nicholls, 1984). In this study, we loosely define a decoupled boundary layer as any layer that is not well-mixed, and often refer to a well-mixed layer as being coupled. Nicholls (1984) used a diagnostic MLM to demonstrate that correctly accounting for decoupling is necessary for a model to adequately reproduce the observed diurnal cycle of stratocumulus.

Published by Copernicus Publications on behalf of the European Geosciences Union.

Decoupling is driven by a number of factors that promote internal stratification of the boundary layer (Bretherton and Wyant, 1997). Daytime insolation drives diurnal decoupling by heating the cloud layer much more than the underlying subcloud layer (e.g. Nicholls, 1984; Turton and Nicholls, 1987). The measurements considered in the current study occur primarily in the morning, so direct diurnal forcing is not the dominant mechanism we observe. Precipitation, even when it mainly evaporates before reaching the surface, promotes "drizzle decoupling" by heating the cloud layer and cooling the subcloud layer. It can be important even in thin cloud layers when cloud condensation nuclei are sparse. Deepening-warming decoupling, introduced by Bretherton and Wyant (1997), can occur as a well-mixed stratocumulus-capped boundary layer deepens by advecting over warmer sea surface temperature (SST). As the layer deepens, increasing latent heat fluxes increase buoyancy production of turbulence in the cloud layer and (through entrainment feedback) drive buoyancy fluxes negative in the subcloud layer until decoupling results.

Our goal in this manuscript is to classify the extent of decoupling observed during the VOCALS Regional Experiment (VOCALS-REx) in October–November 2008, which sampled the Southeast Pacific marine boundary layer off the coast of Chile. This region is home to a large and persistent subtropical stratocumulus deck. As summarized by Bretherton et al. (2010), near the coast the boundary layer is typified by a strong (10–12 K) capping inversion with a typical depth of approximately 1000 m and a typical cloud droplet number concentration of 250 cm^{-3}, while 1500 km to the west the typical depth is 1600 m and the typical cloud droplet concentration is less than 100 cm^{-3}. The boundary layer tends to be well-mixed and non-drizzling near the shore, with a greater tendency to decouple and drizzle further offshore.

This study is based on measurements from 13 research flights (RFs) of one of the two VOCALS long-range aircraft, the NSF C-130. The C-130 sampled from 70°–85° W between 17° and 30° S, with most measurements occurring from pre-dawn to mid-afternoon. A typical RF consisted of a repeated sequence of level legs, including a subcloud leg (150 m above sea level), an in-cloud leg (slightly under the capping inversion), and an above-cloud leg (100–300 m above the inversion), with regular deep profiles extending from 150 m up to 3000 m. See Wood et al. (2011) for a more complete description of VOCALS-REx.

Figure 1 shows a time-height section of reflectivity from the vertically-pointing beams of the University of Wyoming Cloud Radar (WCR) for RF04, a typical flight surveying the boundary layer structure along 20° S. This illustrates the VOCALS flight plan as well as commonly-observed features of the boundary layer structure in the region. It can be compared with a similar figure for RF03 in Bretherton et al. (2010). The C-130 flight path is shown in grey; a radar dead zone is visible around the flight path. The flight starts near the shore, where the nocturnal boundary layer is well-mixed, nondrizzling, and shallow, with an inversion around 1200 m. As the flight proceeds to the west, the inversion height rises, drizzle increases, organized in mesoscale cells, and the boundary layer becomes decoupled, as indicated by the divergence of the LCL based on in-situ measurements, shown in green, and the University of Wyoming Cloud Lidar (WCL) cloud base measured from an upward pointing lidar during subcloud legs flown at approximately 150 m a.s.l. (black). During the return flight from 85° W to the coast the boundary layer again becomes shallower and coupled near the coast, even though it is now nearly noon local time.

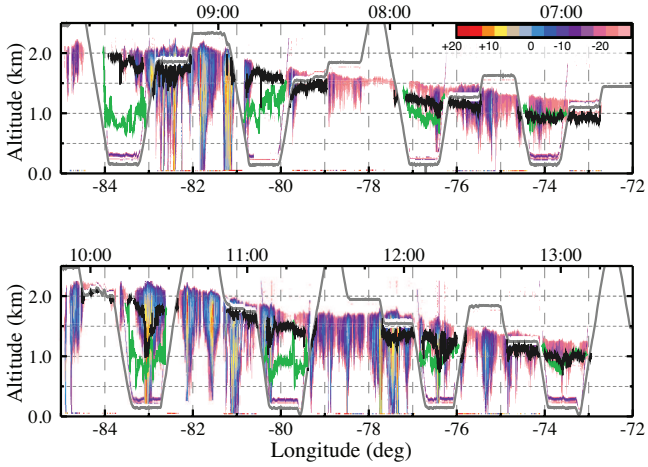

Fig. 1. Time-height sections of RF04 WCR 94 GHz cloud radar reflectivity (dBZ scale shown in the upper right of the top panel). Top panel: outbound flight, bottom panel: return flight. Lidar cloud base during subcloud legs is shown in black, LCL from in-situ measurements is shown in green, and flight path is shown in grey.

The many C-130 flights during VOCALS-REx provide a rich database with which to study decoupling across a range of boundary layer types. In-situ thermodynamic profiles and radar/lidar measurements from subcloud legs provide complementary views of decoupling. Our goal is to use this dataset to statistically characterize decoupling and its relation to cloud cover and thickness, precipitation, and inversion jumps during VOCALS-REx.

2 Decoupling measures and data sources

2.1 Data sources

This analysis utilizes measurements made by the NSF C-130 aircraft and recorded at 1 Hz. In addition to in-situ atmospheric state measurements, we also utilize the WCR to deduce the cloud top and column-maximum radar reflectivity (a precipitation proxy). WCL-derived measurements of cloud base are used during subcloud legs.

The NSF C-130 measurement data are publicly available on the VOCALS Project web page managed by

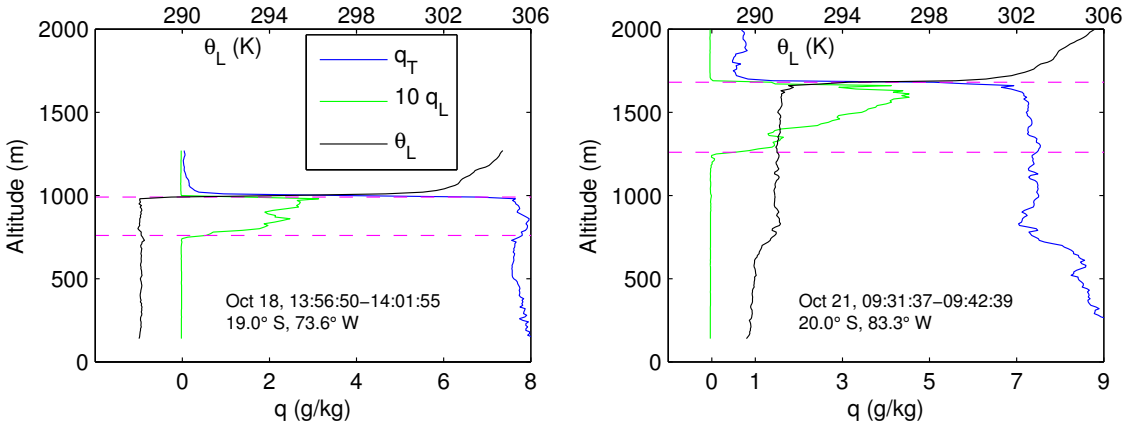

Fig. 2. Typical well-mixed (left) and decoupled (right) profiles of moist-conserved variables. For ease of viewing, 10 times q_ℓ is plotted in green. The dashed magenta lines demarcate the cloud layer.

NCAR/EOL[1]. WCR and WCL data used in this study will also soon become publicly archived at this site. Wood et al. (2011) discusses data availability and access in further detail, along with a summary of the various measurements taken by each of the aircraft that took part in VOCALS-REx.

For ease of comparison, the profile data were averaged within 10 m vertical bins. Corrections to the humidity, measured using the NSF C-130 Lyman-alpha hygrometer, have been applied following Bretherton et al. (2010). These corrections primarily impact the derived LCL, and increase the measured vapor mixing ratio by approximately 5%.

2.2 Profile-based decoupling measure

We use two complementary methods for identifying a decoupled versus well-mixed boundary layer, one of which applies to the profiles while the other utilizes the subcloud legs.

The profile-based method compares the values of θ_ℓ and q_T near the surface to those just below the inversion, providing a direct, local means of interpreting the vertical structure of the boundary layer with regards to decoupling.

Figure 2 shows a typical well-mixed (left) and decoupled (right) profile from VOCALS-REx. In the well-mixed case, the total water mixing ratio q_T and liquid potential temperature θ_ℓ remain relatively constant with height below the inversion. In the decoupled case, there appear to be two well-mixed layers, separated by a 100 m deep stable layer centered at an altitude of 700 m.

Our profile measure of decoupling seeks to capture this behavior by defining moisture and temperature decoupling metrics

$$\Delta q = q_{\text{bot}} - q_{\text{top}}, \tag{3}$$

$$\Delta\theta_\ell = \theta_{\ell,\text{top}} - \theta_{\ell,\text{bot}} \tag{4}$$

[1]http://www.eol.ucar.edu/projects/vocals/dm/index.html

where the subscript "bot" denotes the mean over the bottom 25 % of the boundary layer below the inversion, and "top" the mean over the top 25 % of the boundary layer below the inversion. For each profile the height of the inversion, z_i, is determined as the height at which the temperature is a minimum provided the relative humidity is at least 45 %. We use 110 C-130 profiles during VOCALS-REx that extend from below $0.25z_i$ through the inversion, and that lie north of 25° S. Two coastal aerosol flights went south of 25° S, where they sampled a shallow boundary layer under strong synoptically-driven subsidence with a diffuse inversion and patchy cloud cover atypical of the rest of the VOCALS region considered in this study.

With regards to moisture, we identify profiles with $\Delta q > 0.5\,\text{g}\,\text{kg}^{-1}$as decoupled. This threshold is somewhat arbitrary, but seems to differentiate between those profiles which have a distinct humidity decrease just above the LCL (Fig. 2b) from those that do not. A proportional least-squares fit between Δq and $\Delta\theta_\ell$ suggests that $\Delta q = 0.5\,\text{g}\,\text{kg}^{-1}$corresponds to $\Delta\theta_\ell = 0.5\,\text{K}$. Thus, we identify profiles with $\Delta q < 0.5\,\text{g}\,\text{kg}^{-1}$and $\Delta\theta_\ell < 0.5\,\text{K}$ as well-mixed, and all other profiles as decoupled.

Figure 3 shows a scatter plot in Δq and $\Delta\theta_\ell$ of the profile decoupling metric for the REx profiles included in this analysis. The well-mixed threshold is indicated on the plot by the box in the lower left corner, and the least-squares fit between Δq and $\Delta\theta_\ell$ is shown by the dashed black line. Approximately 28 % of profiles in VOCALS-REx were classified as well-mixed.

Figure 4 shows composite profiles from the VOCALS-REx dataset based on the degree of decoupling indicated by Δq (i.e., without the $\Delta\theta_\ell$ restriction). For each profile, the mean LCL was calculated from the bottom 25 % of the boundary layer. For the composited profiles, the profiles were scaled so each LCL and z_i aligned. The composite mean was then rescaled so that the dashed black line

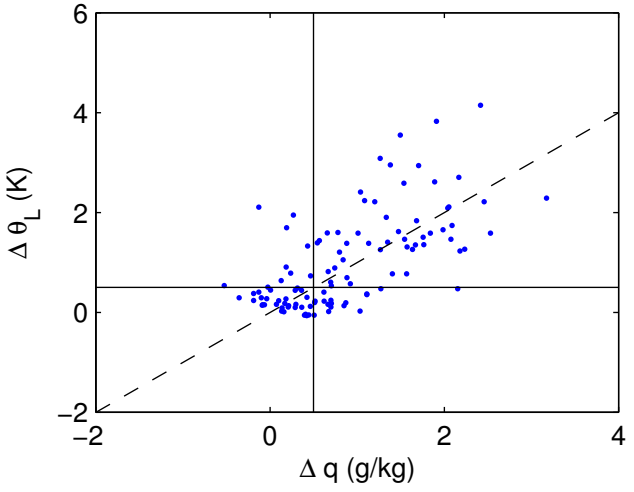

Fig. 3. Scatter plot of $\Delta\theta_\ell$ versus Δq with the "well-mixed" classification indicated by the lower left box. The least-squares best linear fit passing through the origin is denoted by the dashed line.

indicates the mean z_i for each subset of profiles included in the composite, and the dashed red line the mean LCL.

The composite profiles in Fig. 4 share many of the features of the coupled and decoupled composite profiles from the PACS Stratus 2004 cruise presented in Serpetzoglou et al. (2008). In the well-mixed panel (top), the inversion is lower than in the decoupled profiles, the LCL coincides with the cloud base, and q_ℓ within the cloud increases linearly with height up to the inversion. As the degree of decoupling increases, the boundary layer deepens, the difference between z_i and the LCL increases, and the LCL diverges from the cloud base, while the stratiform cloud thickness remains relatively unchanged.

2.3 Subcloud decoupling measure Δz_b

Another "subcloud" measure of decoupling is provided by the C-130 subcloud legs flown at approximately 150 m above sea level, based on comparison of the the aircraft-measured LCL and the WCL-measured cloud base z_b on these legs. When the boundary layer is well-mixed, the LCL and cloud base measurements are in close agreement, but in the decoupled regime the LCL and cloud base may diverge by as much as several hundred meters (see Fig. 4).

Figure 5 shows the LCL and cloud base measurements for the subcloud legs adjacent to the profiles in Fig. 2. In the well-mixed case (left) the LCL and cloud base are close; their difference fluctuates around 50 m (this value is sensitive to humidity calibrations applied to the data and should be regarded as having a roughly 50 m uncertainty; see Bretherton et al., 2010). Their "mesoscale" variability also correlates well (here mesoscale refers to scales much longer than 10 s of flight time, which at the 100 m s^{-1} nominal aircraft speed

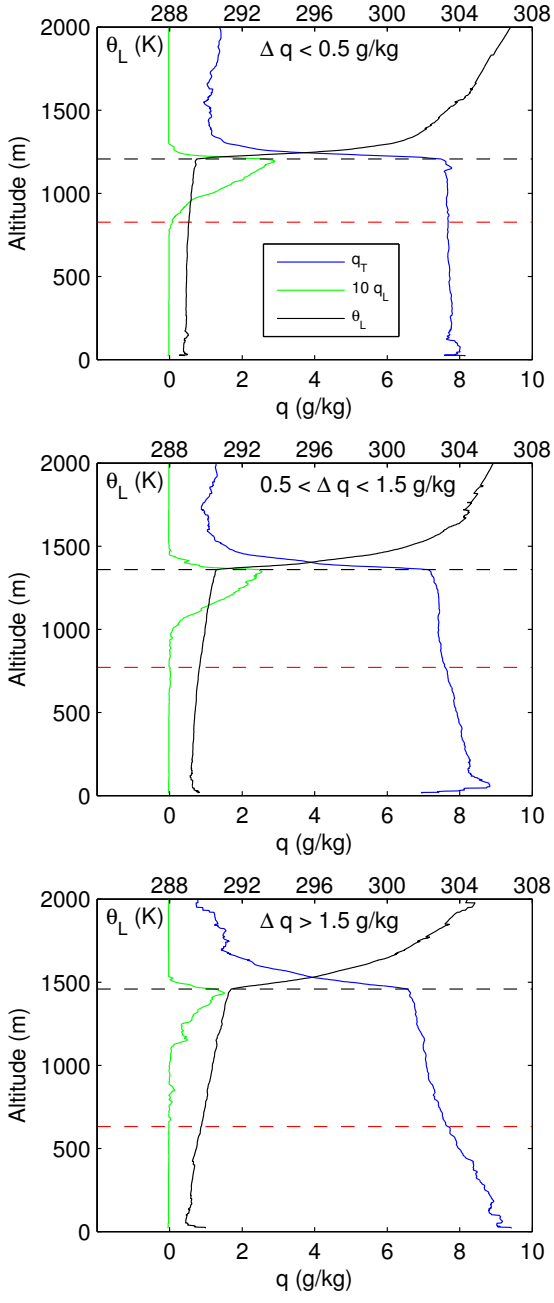

Fig. 4. Composite VOCALS-REx profiles for $\Delta q < 0.5\,\mathrm{g\,kg^{-1}}$ (top), $0.5 < \Delta q < 1.5\,\mathrm{g\,kg^{-1}}$ (center), and $\Delta q > 1.5\,\mathrm{g\,kg^{-1}}$ (bottom). The mean inversion is indicated by the dashed black line, and the mean LCL, determined from the bottom 25 % of the boundary layer, is demarcated by the dashed red line.

corresponds to distances much longer than 1 km). By contrast, the decoupled case (right) shows tremendous variability in both the LCL and WCL cloud base. The difference between the cloud base and the LCL ranges between 100 and 1000 m across the 700 s (70 km) leg.

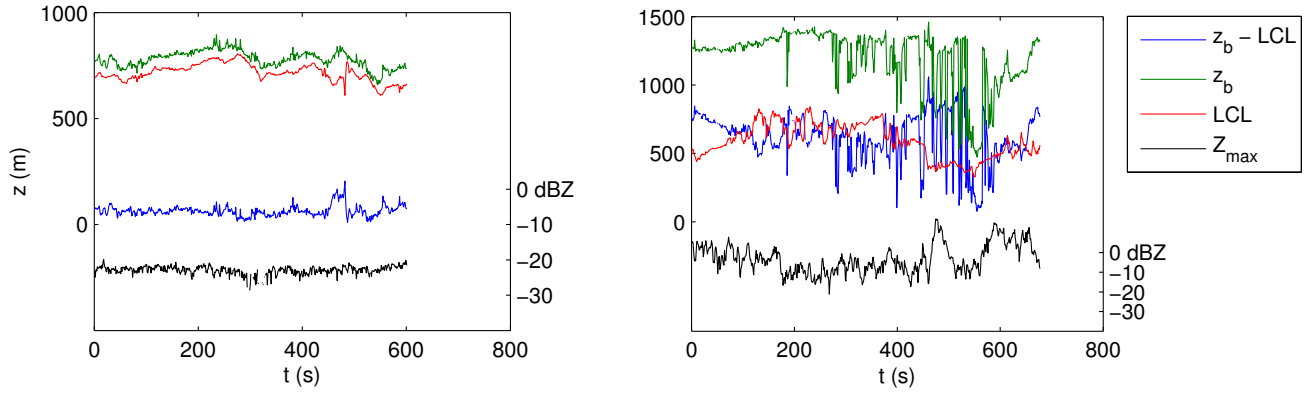

Fig. 5. Cloud base and LCL of the subcloud legs adjacent to the profiles shown in Fig. 2, showing an example of the mesoscale structure associated with a well-mixed (left) and decoupled (right) boundary layer.

A subcloud decoupling index was computed for each subcloud leg as the leg-mean difference between the z_b and the LCL:

$$\Delta z_b = \overline{z_b - z_{\mathrm{LCL}}}. \tag{5}$$

2.4 Relation between Δq, $\Delta\theta_\ell$, and Δz_b

A Δz_b threshold for decoupling that is consistent with the profile-based Δq and $\Delta\theta_\ell$ thresholds can be derived from a thermodynamic argument. The LCL is based on the aircraft measured temperature, pressure, and moisture during a subcloud leg flown at an altitude of $z_{\mathrm{SC}} \approx 150$ m. Thus, the saturation mixing ratio $q^*(p_{\mathrm{LCL}}, T_{\mathrm{LCL}}) = q_v(z_{\mathrm{SC}})$, where p_{LCL} and T_{LCL} are the temperature and pressure derived by dry-adiabatically lifting mean subcloud-layer air to the height z_{LCL}. On the other hand, the cloud base z_b is the exact level at which the air becomes saturated, so $q_v(z_b) = q^*(p_b, T(z_b))$.

To compare the two metrics, we neglect the weak dependence of q^* on pressure, by approximating the true pressure with a reference pressure p_0 close to the true cloud base and LCL pressures. We assume that the cloud base humidity is approximately equal to the mean q_T over the top 25 % of the boundary layer, and that $q_v(z_{\mathrm{SC}})$ is approximately equal to the humidity averaged over the bottom 25 % of the boundary layer below the inversion. Then

$$\begin{aligned}\Delta q &\approx q_v(z_{\mathrm{SC}}) - q_v(z_b) \\ &= q^*(p_{\mathrm{LCL}}, T_{\mathrm{LCL}}) - q^*(p_b, T_{\mathrm{da}}(z_b)) \\ &- [q^*(p_b, T(z_b)) - q^*(p_b, T_{\mathrm{da}}(z_b))] \\ &\approx -\left(\frac{dq^*}{dz}\right)_{\mathrm{da}} (z_b - z_{\mathrm{LCL}}) - \left(\frac{\partial q^*}{\partial T}\right) (\theta_\ell(z_b) - \theta_\ell(z_{\mathrm{LCL}})).\end{aligned} \tag{6}$$

Here the subscript "da" indicates a dry-adiabatic and hydrostatic vertical displacement from the LCL.

Rearranging Eq. (6) yields

$$\Delta z_b \approx \frac{1}{-(dq^*/dz)_{\mathrm{da}}} \left(\Delta q + \left(\frac{\partial q^*}{\partial T}\right)_{\mathrm{LCL}} \Delta\theta_\ell\right). \tag{7}$$

At a characteristic boundary layer pressure of 950 hPa and temperature of 285 K, and $\Delta\theta_\ell/\Delta q = 1\,\mathrm{K\,kg\,g^{-1}}$ as in our profile well-mixed criteria, Eq. (7) implies that $\Delta q = 0.5\,\mathrm{g\,kg^{-1}}$ corresponds to $\Delta z_b \approx 166$ m. Bearing in mind the approximations made in deriving Eq. (7) and the uncertainty in the measured Δz_b, we find a threshold of 150 m is appropriate. Hence, a subcloud leg is considered well-mixed if $\Delta z_b < 150$ m and decoupled otherwise.

Figure 6 shows the consistency of the Δq and Δz_b measures. In this figure, Δq for each profile with an adjacent (occurring within 5 min) subcloud leg are matched with the corresponding Δz_b. The dashed black line indicates the linear relationship $\Delta z_b/\Delta q = 150\mathrm{m}/(0.5\ \mathrm{g\ kg^{-1}})$ obtained from the thermodynamic argument. As expected, there is a strong correlation between Δq and Δz_b; some scatter is expected because Δq comes from a single profile while Δz_b is an average over a leg that is near to the profile but does not overlap it, and because there is some variability in the temperature lapse rate beneath the cloud base.

2.5 Decoupling vs. drizzle from the subcloud legs

The subcloud legs are long enough to meaningfully characterize the average cloud-base precipitation. Since the precipitation of drizzle-size and larger droplets in drizzling stratocumulus typically maximizes near the cloud base, we use as a drizzle proxy the leg-mean of the maximum cloud radar reflectivity Z_{max} in the boundary-layer column above the aircraft (sampled at 1 Hz), converted to a decibel scale:

$$dBZ = 10\log_{10}(\overline{Z_{\mathrm{max}}}). \tag{8}$$

We define $dBZ > 0$ as heavy drizzle, $-10 < dBZ < 0$ as light drizzle, and $dBZ < -10$ as no (i.e. negligible) drizzle.

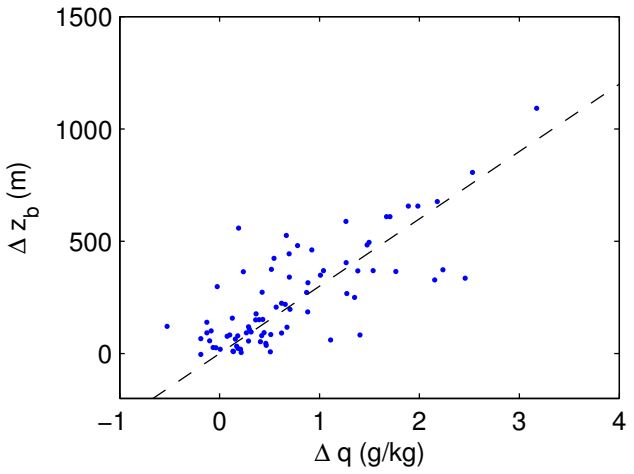

Fig. 6. The profile moisture decoupling index Δq and the decoupling measurement from the adjacent subcloud leg Δz_b are consistent metrics for determining decoupling. The dashed black line has slope 150 m per 0.5 (g kg^{-1}).

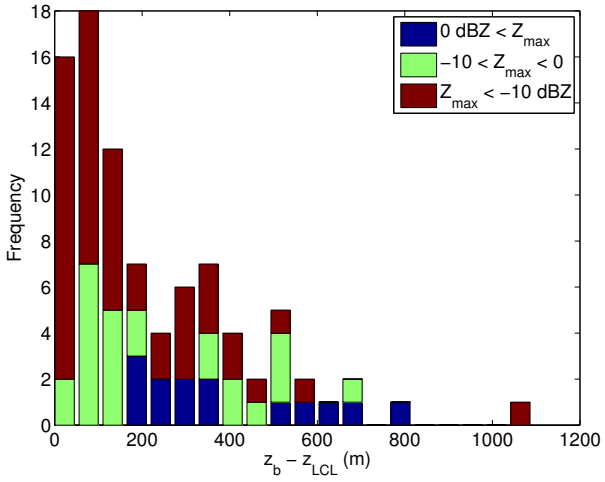

Fig. 7. Mean cloud base – LCL (Δz_b) for each subcloud leg. Each bin is also separated based on drizzle.

Figure 7 shows a histogram of the subcloud decoupling metric for all C-130 subcloud legs during VOCALS-REx, categorized by drizzle intensity. Approximately 45 % of subcloud legs are found to have $\Delta z_b < 150$ m, in reasonable agreement with the fraction of well-mixed profiles. There is some correlation between decoupling and drizzle; in particular all heavily drizzling regions are classified as decoupled.

3 Correlation of decoupling with boundary-layer characteristics

The best correlate we found for decoupling in the REx dataset is the "mixed layer cloud thickness" $\Delta z_M = \overline{z_i - z_{\mathrm{LCL}}}$, the thickness the cloud layer would have if the boundary layer was well-mixed and had the thermodynamic characteristics of the subcloud layer.

One might expect that the mixed layer cloud thickness would correlate with decoupling based on arguments of Bretherton and Wyant (1997). Consider two cloud-topped mixed layers with identical z_i and θ_ℓ, one of which is slightly moister than the other so as to support a thicker cloud layer. The thicker cloud layer generates more entrainment because entrainment is driven by in-cloud turbulence, whose primary source is buoyancy flux integrated over the depth of the turbulent layer. The turbulent buoyancy fluxes are large within the cloud layer because the moist updrafts have more liquid water, whose condensation releases more latent heat, than in the downdrafts. Below the cloud base, latent heating does not add to the buoyancy flux, which can therefore be small or even negative (with strong enough entrainment of warm above-inversion air). Thus, the turbulence is driven by the in-cloud contribution to vertically integrated buoyancy flux, which increases in proportion to cloud depth. Hence, a thicker cloud layer will produce more turbulence and entrainment, which favors decoupling.

Figure 8 shows the longitudinal variation of decoupling and drizzle for the subcloud legs plotted versus Δz_M. The mixed layer cloud depth tends to increase from east to west. When Δz_M is shallow, the boundary layer typically remains well-mixed with little to no drizzle. As Δz_M increases above 500 m, the boundary layer tends to decouple and drizzle. Interpreted in this manner, the decoupling of the boundary layer further to the west is associated with larger Δz_M, which in turn reflects the westward increase in inversion height with no corresponding systematic increase in LCL. The relation between mixed layer cloud thickness, drizzle, and decoupling has little longitudinal dependence, even though there is a systematic decrease in boundary-layer accumulation-mode aerosol and cloud droplet concentrations to the west.

Several VOCALS-REx flights were devoted to investigating pockets of open cells (POCs). Even legs within POCs, shown in Fig. 8 as open symbols, which have particularly low droplet concentrations, do not greatly deviate from the longitude-mean trends, although as expected they do seem to have somewhat higher drizzle intensities for a given mixed layer cloud thickness. These results suggest that while aerosol-cloud interactions may modulate decoupling in the VOCALS region, they are not its dominant controlling factor.

Figure 9 shows the longitudinal variation of decoupling using the profiles instead of the subcloud legs. The LCL was determined as an average value from the bottom 25 % of the boundary layer. The general features are similar to those shown in Fig. 8 for the subcloud leg, but the separation between the well-mixed and decoupled legs is not nearly as sharp. This is to be expected, since the subcloud

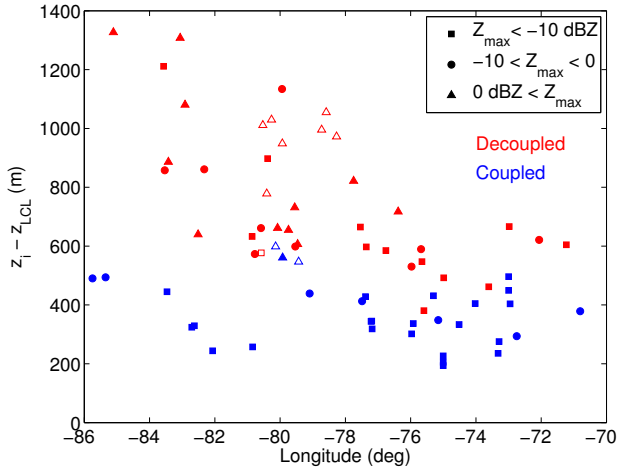

Fig. 8. Decoupling, mixed layer cloud thickness Δz_M, and drizzle by longitude for each subcloud leg. Blue (red) markers indicate well-mixed (decoupled) legs. Moderately drizzling legs are indicated by triangles, lightly drizzling legs by circles, and nondrizzling legs by squares. POC legs are indicated by hollow markers.

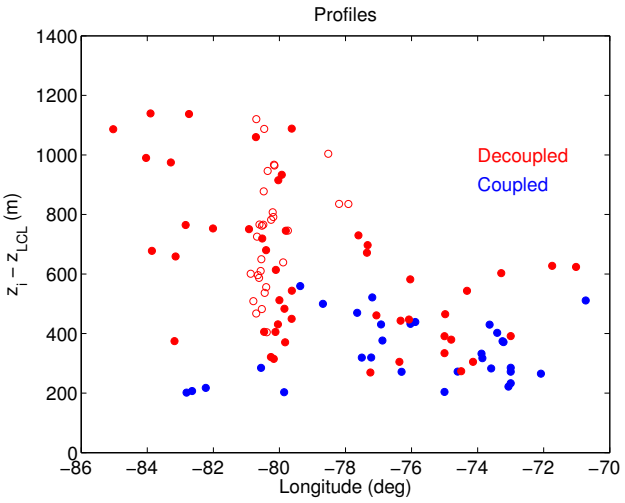

Fig. 9. Decoupling and mixed layer cloud thickness Δz_M by longitude for each profile. Blue (red) markers indicate well-mixed (decoupled) profiles. POC profiles are indicated by the hollow markers.

measurements are based on leg means (and as such capture the averaged properties over approximately 60 km), whereas the profiles are based on a single ascent or descent, which is more susceptible to local fluctuations.

The profiles are not categorized by drizzle intensity since the uncertainty in measuring the maximum radar reflectivity from the cloud base due to the radar direction and radar dead zone during profiles renders the measurements significantly less meaningful than the corresponding subcloud measurement of dBZ.

The VOCALS-REx research flights occurred mainly during the morning, and span too limited a range of times of day to usefully study the diurnal variation of decoupling in the VOCALS region; in fact we had difficulty detecting a diurnal signature of decoupling at any longitude using our two measures and dataset.

Our findings are qualitatively consistent with the deepening-warming mechanism for decoupling described in Bretherton and Wyant (1997). Using a mixed layer model, the authors identify the surface latent heat flux (LHF), net radiative flux divergence across the boundary layer ΔF_R, and z_b/z_i as important quantities controlling the onset of decoupling. In particular, for the highly idealized case of a steady-state, non-precipitating, well-mixed stratocumulus-capped boundary layer, they obtained the following condition for the development of a layer of negative subcloud buoyancy flux necessary for decoupling to occur:

$$\frac{\Delta F_R}{\mathrm{LHF}} < A\eta\frac{\Delta z_M}{z_i}, \tag{9}$$

where A is the entrainment efficiency, and $\eta \approx 0.9$ is a thermodynamic variable. Based on an analysis of earlier ship-based observations in the VOCALS region, Caldwell et al. (2005) inferred $A \approx 1.1$. Precipitation, horizontal advection, heat storage and other characteristics of the boundary layer can be accounted for as correction terms to ΔF_R in Eq. (9) (Bretherton and Wyant, 1997). These correction terms may well be at least as large as ΔF_R itself, but they are difficult to reliably estimate from the available data, preventing us from making a precise comparison of the model with the VOCALS observations. However, we can use Eq. (9) as a framework for interpreting the role of different environmental factors in the decoupling observed in VOCALS-REx.

For the inferred $A = 1.1$, the right-hand side of Eq. (9) is approximately equal to $\Delta z_M/z_i$. That is, the decoupling criterion is more likely to be satisfied if $\Delta z_M/z_i$ is larger, consistent with the results of $\Delta z_M/z_i$ ranges shown in Fig. 8. A typical value of $\Delta z_M/z_i$ ranges from 0.3 for subcloud legs near the coast to 0.6 for legs at 85° W.

We also have attempted to evaluate the left hand side of Eq. (9). The overall result is that in the VOCALS dataset, it is significant but less important in regulating decoupling than is $\Delta z_M/z_i$, and tends to act in the same sense of promoting more decoupling further to the west.

The LHF was estimated using a bulk aerodynamic relationship

$$\mathrm{LHF} = \rho_{\mathrm{ref}} L C_T V (q_{ts} - q_{tM}), \tag{10}$$

where $C_T \approx 0.001$ is a transfer coefficient, V is the mean horizontal wind speed during a 150 m subcloud leg, q_{ts} is the water saturation mixing ratio at SST (multiplied by 0.981 to account for ocean salinity), q_{tM} is mixed layer mixing ratio, taken to be the leg-mean q_T, and ρ_{ref} is a reference air density. When binned into 5° longitude ranges 70°–75° (near shore), 75°–80°, and 80°–86° W (far west), the mean LHF

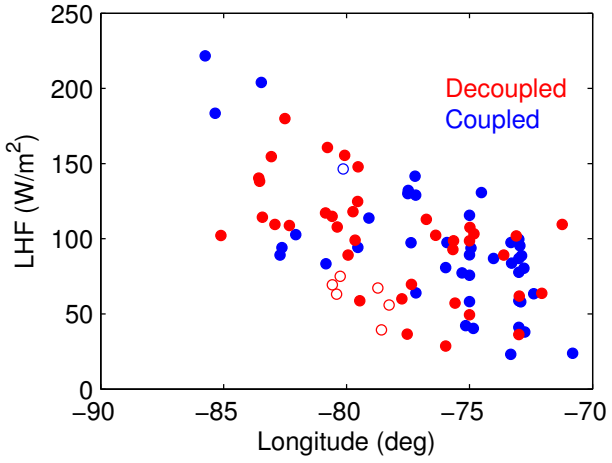

Fig. 10. Latent heat flux by longitude for each subcloud leg. Blue (red) markers indicate well-mixed (decoupled) subcloud legs. Hollow markers indicate POC legs.

increases from 72 W m^{-2} near shore to 126 W m^{-2} in the far west, an increase of 75 %. The increase of LHF to the west tends to further promote decoupling, since an increase in LHF leads to an increase in the cloud base buoyancy flux jump (Bretherton and Wyant, 1997).

The radiative flux divergence across the boundary layer, measured on a leg-by-leg basis following the approach of Bretherton et al. (2010), and accounting for both longwave and shortwave flux, also increases to the west. When the data are binned longitudinally, the flux divergence increases by nearly the same factor as the LHF, and the average ratio $\Delta F_R/\mathrm{LHF} \approx 0.4$–$0.65$. However, this is biased somewhat by the flight plan, in which the near shore region is sampled both in the early morning on the outbound flights, and later in the day on the return trip when shortwave forcing is significant, while the far west region is sampled primarily in the early morning. When the sample is restricted to morning (before 09:00 local time), non-precipitating legs (for which the expression given by Eq. (9) is most applicable), the LHF increases from 70 W m^{-2} near shore to 135 W m^{-2} offshore, while ΔF_R increases from 71 W m^{-2} to 95 W m^{-2}, a much less significant increase than the LHF. Based on these arguments, the left-hand side of Eq. (9) typically ranges from 1 near the coast to 0.7 at 85° W, and the typical ratio of the right hand side to the left hand side varies from 0.3 near the coast to 0.9 at 85° W. A ratio of 0.4 roughly corresponds to the observed decoupling threshold. The idealized model suggests this threshold ratio should be the larger value of 1, a discrepancy probably due to the terms neglected in Eq. (9). However, the idealized model does correctly predict that decoupling should be much more common further offshore, and also correctly predicts that the variation of $\Delta z_M/z_i$ is the most important factor modulating this tendency.

Accounting for the effects of precipitation, diurnal variability, and horizontal advection might help bring the Bretherton and Wyant (1997) model into better quantitative agreement with the data.

The idealized model suggests that for fixed $\Delta z_M/z_i$, increased LHF might help induce decoupling. Figure 10 shows our bulk estimate of LHF vs. longitude, with decoupled legs colored in red. In contrast to Fig. 8, there is no clear separation of well-mixed from decoupled legs at any given longitude. It is thus our interpretation that although there is a correlation between LHF and decoupling, LHF does not play the dominant role in determining decoupling in VOCALS-REx. In fact, no other combination of parameters appearing in Eq. (9) is able to reliably classify a decoupled profile as well as Δz_M.

3.1 Inversion jumps

Past studies have suggested jumps of moist thermodynamic properties between the inversion base and top are an important control on stratocumulus entrainment, cloud fraction and decoupling. Randall (1980) hypothesized that if these jumps supported the production of negatively buoyant mixtures of cloudy and above-inversion air ("buoyancy reversal"), a runaway cloud-top entrainment instability would evaporate the cloud; this process would also decouple the boundary layer due to the strong associated downward entrainment flux of warm air below cloud base. While prior field observations have shown frequent examples of stratocumulus persisting despite buoyancy reversal (Kuo and Schubert, 1988), they do not rule out more stringent instability criteria that have been proposed since (e.g. MacVean and Mason, 1990). Many stratocumulus entrainment parametrizations build in some enhancement of the efficiency of entrainment with increasing buoyancy reversal (e.g. Nicholls and Turton, 1986; Lock, 2000). Recently, a set of large-eddy simulations by Lock (2009) showed a strong relation between stratocumulus cloud cover and a ratio of inversion humidity and temperature jumps

$$\kappa = 1 + \frac{\delta\theta_\ell}{(L/c_p)\delta q_T}, \tag{11}$$

where δx indicates the difference between x just above the inversion and just below the inversion. κ provides a measure of the buoyancy of air parcels at the cloud top formed by mixing cloudy air with air from just above the inversion, and is thus related to the entrainment rate. Buoyancy reversal occurs for $\kappa > 0.23$ and becomes more pronounced for larger κ. The large-eddy simulations presented by Lock (2009) maintained solid stratocumulus cover for $\kappa < 0.4$, with a smooth transition for $0.4 < \kappa < 0.5$ to cloud fractions less than 20%.

We examined the relationship between inversion jumps, cloud fraction, and decoupling in the REx C-130 profile dataset. The top of the entrainment zone was identified as the minimum height above the inversion for which both the

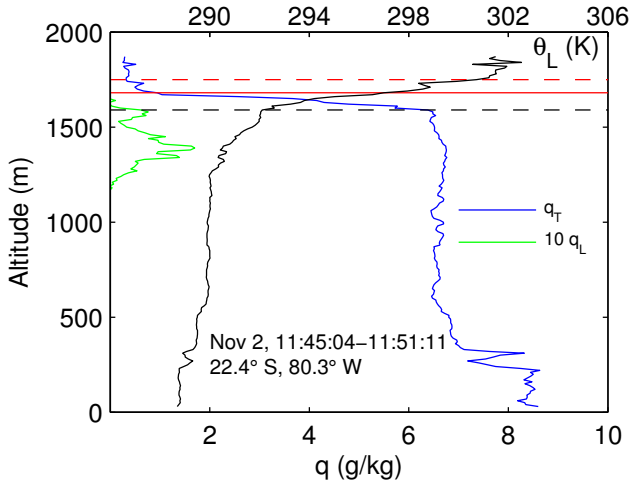

Fig. 11. Liquid water mixing ratio (green), total water mixing ratio (blue), and liquid potential temperature (black) profiles illustrating the inversion structure observed in a typical POC profile. The dashed black line marks the inversion base. The inversion top deduced using the criteria described in Sect. 3.1 is indicated by the solid red horizontal line, whereas the visually determined inversion top used to calculate κ is indicated by the dashed red line.

relative humidity and temperature gradients remained sufficiently small ($\left|\frac{d\mathrm{RH}}{dz}\right| < 0.3\ \%\,\mathrm{m}^{-1}$, $\frac{d\theta_\ell}{dz} < 0.1\,\mathrm{K\,m}^{-1}$) for a vertical range of 100 m, and the relative humidity was within 10 % of the profile-minimum. This procedure works well for identifying the entrainment zone when the capping inversion is sharp, as is typical in VOCALS-REx (for example, see Fig. 2).

Within POCs, however, the entrainment zone tends to be thicker and the inversion more diffuse, resulting in a more complex inversion structure for which this approach is insufficient to adequately identify the inversion jump. Figure 11 shows the inversion structure from a sample POC profile. The inversion top identified by the above method, shown as a solid red line, does not extend high enough to capture the full moisture and temperature jump. Thus, for POC profiles we instead determine the inversion top visually, choosing the height which best reflects the temperature and moisture in the free troposphere. The dashed red line marks the visually-identified inversion top that was used to calculate κ for this profile.

For each profile that had an adjacent subcloud leg, we calculated a lidar-derived cloud fraction averaged over the 10 minutes of the subcloud leg closest to the profile. To control for the strong diurnal cycle of cloud fraction, we restricted cloud fraction measurements to profiles occurring before 10:00 LT.

Portions of several RFs were devoted to investigating POCs, and the flight plan of these flights required a more sophisticated approach to link POC profile and subcloud leg for

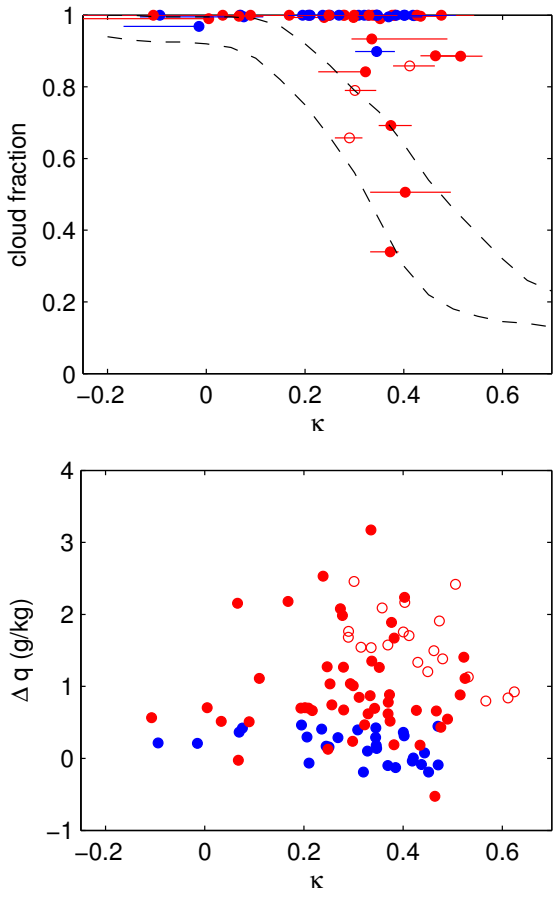

Fig. 12. Cloud fraction (top) and profile moisture decoupling index (bottom) as a function of the inversion jump parameter κ. Well-mixed profiles are marked in blue, and decoupled profiles in red. Data from POC flights are shown as hollow markers. Only profiles with adjacent subcloud legs before 10:00 LT are included in the left panel to reduce the influence of diurnal forcing on the cloud fraction. Uncertainty estimates for κ are indicated by bars in the left panel, and the dashed curves correspond to the range of LES results presented in Lock (2009).

determining the cloud fraction, to ensure that both the profile and subcloud leg were within the POC region. The flight plan was such that there was typically only one morning subcloud leg that extended into the POC, with several POC profiles. For each POC subcloud leg, we identified the region that was within the POC using GOES-10 thermal infrared satellite images from the time of the subcloud leg, and then found the nearest spatially collocated POC profile. Before 10:00 LT, there are only 3 POC profiles associated with a subcloud leg, occurring in RF07-RF09. Missing from these is RF06, the POC flight featured in Wood et al. (2010). We were unable to reliably determine the inversion jumps from RF06 because the fast-response Lyman-alpha hygrometer was inoperative on this flight.

Figure 12 shows scatter plots between κ, cloud fraction and Δq in the C-130 profile dataset. The bottom panel suggests that decoupling is not correlated to κ unless κ is very large. For $\kappa > 0.48$, all measured profiles were decoupled. Among the pre-10:00 LT profiles with which we can associate a cloud fraction, it is 100 % for most cases, and in almost all cases with $\kappa < 0.25$. However, once κ exceeds approximately 0.3, there are several cases with partial cloud cover, nearly all of which are decoupled. These observations are qualitatively consistent with the large-eddy simulation results presented in Lock (2009), though the observed cloud fraction tends to be somewhat larger at a given κ than the range suggested by the simulations, which is shown by the pair of dashed curves. The agreement is improved by considering only decoupled profiles, which is most consistent with the cumulus under stratocumulus regime presented in Lock (2009), although there are decoupled profiles with nearly 100 % cloud cover for κ up to 0.5.

The κ parameter is sensitive to the identified inversion jump. To estimate the uncertainty range for κ, we determined the minimum and maximum κ calculated shifting both the inversion top and bottom through a range of ± 20 m. This range is depicted by the error bars in the top panel of Fig. 12.

Data points from profiles within POCs are indicated by hollow markers in Fig. 12. From the bottom panel we gather that the POC regions were all decoupled with $\kappa > 0.28$. The three POC profiles with a corresponding cloud fraction are plotted in the top panel. These fall on the low edge of the non-POC profiles, consistent with cloud-aerosol-precipitation feedbacks reducing cloud fraction in POCs compared to surrounding stratocumulus with similar inversion jumps.

4 Conclusions

We used profiles and subcloud legs from VOCALS-REx to classify each leg as well-mixed or decoupled. We find that the well-mixed boundary layer tends to be shallow ($z_i \approx 1200$ m), non-drizzling, and with nearly solid cloud cover. The decoupled boundary layer tends to be deeper ($z_i \approx 1400$ m), with increased drizzle occurance and decreased cloud fraction relative to the coupled boundary layer. The observed cloud was typically 280–350 m thick, and did not vary significantly between well-mixed and decoupled profiles.

We also find that decoupled profiles tend to have higher horizontal wind speed in the boundary layer, and contain more moisture in the surface layer and less in the cloud layer than their well-mixed counterparts. These findings generally support those of the PACS Stratus 2004 mission presented in Serpetzoglou et al. (2008), although we observe substantially increased drizzle occurance in decoupled subcloud legs (54 % of decoupled subcloud legs were drizzling, compared to 21 % of the well-mixed legs), and a smaller difference in mean cloud fraction (96 % for well-mixed legs, compared to 91 % for decoupled legs). These differences are likely due to a combination of the variability of conditions in the southeast Pacific, and the lack of measurements sampling diurnally-driven decoupling in the current study.

We find the mixed layer cloud thickness Δz_M to be the best predictor for decoupling observed in VOCALS-REx. This is shown most strikingly by the sharp distinction between the range of values of Δz_M for coupled and decoupled subcloud legs in Fig. 8, in which legs are typically decoupled when $\Delta z_M > 500$ m, and well-mixed otherwise.

This empirical threshold for decoupling occurs at approximately the same cloud thickness where precipitation can be expected to become significant. Similarly, we also note that LHF, another factor in driving boundary layer decoupling, increases to the west along with the prevalence of decoupling. Each of these mechanisms likely plays an important role in decoupling in VOCALS-REx. However, no other parameter is able to predict decoupling as consistently as Δz_M.

The identified relationship between Δz_M and decoupling is important and appealing because it is concise, robust, and qualitatively consistent with prior theoretical arguments. It suggests that, at least within the VOCALS region, boundary layer deepening is the principal control on decoupling even though other mechanisms may contribute. It also supports the use of bulk mixing-line models of boundary layer structure, such as Park et al. (2004), which divide the boundary layer into a well-mixed layer extending up to cloud base and a cloud layer in which the gradients of q_T and θ_ℓ depend on the cloud layer thickness Δz_M.

In general, the inversion jump parameter κ was found not to be a good predictor of decoupling. Coupled and decoupled profiles are well-distributed across the range of κ values. The only exception to this is for very large values of κ. Though it represents a small sample of points from which no definitive conclusion can be drawn, all 8 profiles with $\kappa > 0.5$ were found to be decoupled. Most of these profiles were within POCs.

While κ is not a good predictor for decoupling, we do find that a low cloud fraction is nearly always associated with a high κ and decoupling. Decoupling in itself, however, is not a good predictor for low cloud fraction or large κ, and many subcloud legs classified as decoupled were nearly 100 % cloud covered.

Acknowledgements. The authors gratefully acknowledge support from NSF grant ATM 0745702 (CB) and ATM-0745986 (DL) and a Boeing Endowed Professorship in Applied Mathematics awarded to CB. The RAF C-130 measurements were obtained from the VOCALS data archive of NCAR/EOL, which is sponsored by the NSF. Chris Terai helped prepare the C-130 profile dataset. Rob Wood provided much helpful advice.

Edited by: B. Albrecht

References

Bretherton, C. S. and Wyant, M. C.: Moisture transport, lower-tropospheric stability, and decoupling of cloud-topped boundary layers, J. Atmos. Sci., 54, 148–167, 1997.

Bretherton, C. S., Uttal, T., Fairall, C. W., Yuter, S., Weller, R., Baumgardner, D., Comstock, K., and Wood, R.: The EPIC 2001 stratocumulus study, B. Am. Meteorol. Soc., 85, 967–977, 2004.

Bretherton, C. S., Wood, R., George, R. C., Leon, D., Allen, G., Zheng, X.: Southeast Pacific stratocumulus clouds, precipitation and boundary layer structure sampled along 20 S during VOCALS-REx, Atmos. Chem. Phys., 10, 10639–10654, doi:10.5194/acp-10-10639-2010, 2010.

Caldwell, P., Bretherton, C. S., and Wood, R.: Mixed-layer budget analysis of the diurnal cycle of entrainment in Southeast Pacific stratocumulus, J. Atmos. Sci., 62, 3775–3791, 2005.

Kuo, H. and Schubert, W.: Stability of cloud-topped boundary-layers, Q. J. Roy. Meteorol. Soc., 114, 887–916, 1988.

Lilly, D.: Models of cloud-topped mixed layers under a strong inversion, Q. J. Roy. Meteorol. Soc., 94, 292–309, 1968.

Lock, A., Brown, A.,Bush, M., Martin, G., and Smith, R.: A new boundary layer mixing scheme. Part I: Scheme description and single-column model tests Mon. Weather Rev., 128, 3187–3199, 2000.

Lock, A. P.: Factors influencing cloud area at the capping inversion for shallow cumulus clouds, Q. J. Roy. Meteorol. Soc., 135, 941–952, 2009.

MacVean, M. K. and Mason, P. J.: Cloud-top entrainment instability through small-scale mixing and its parameterization in numerical-models, J. Atmos. Sci., 47, 1012–1030, 1990.

Nicholls, S.: The dynamics of stratocumulus–aircraft observations and comparisons with a mixed layer model, Q. J. Roy. Meteorol. Soc., 110, 783–820, 1984.

Nicholls, S. and Turton, J.: An observational study of the structure of stratiform cloud sheets. 2. entrainment, Q. J. Roy. Meteorol. Soc., 112, 461–480, 1986.

Park, S., Leovy, C., and Rozendaal, M.: A new heuristic Lagrangian marine boundary layer cloud model, J. Atmos. Sci., 61, 3002–3024, 2004.

Randall, D.: Conditional instability of the 1st kind upside-down, J. Atmos. Sci., 37, 125–130, 1980.

Serpetzoglou, E., Albrecht, B. A., Kollias, P., Fairall, C. W.: Boundary layer, cloud, and drizzle variability in the southeast Pacific stratocumulus regime, J. Climate, 21, 6191–6214, 2008.

Turton, J. D. and Nicholls, S.: A study of the diurnal-variation of stratocumulus using a multiple mixed layer model, Q. J. Roy. Meteorol. Soc., 113, 969–1009, 1987.

Wood, R., Bretherton, C.S., Leon,D., Clarke, A. D., Zuidema, P., Allen, G., and Coe, H.: An aircraft case study of the spatial transition from closed to open mesoscale cellular convection over the Southeast Pacific, Atmos. Chem. Phys. Discuss., 10, 17911–17980, doi:10.5194/acpd-10-17911-2010, 2010.

Wood, R., Mechoso, C. R., Bretherton, C. S., Weller, R. A., Huebert, B., Straneo, F., Albrecht, B. A., Coe, H., Allen, G., Vaughan, G., Daum, P., Fairall, C., Chand, D., Gallardo Klenner, L., Garreaud, R., Grados, C., Covert, D. S., Bates, T. S., Krejci, R., Russell, L. M., de Szoeke, S., Brewer, A., Yuter, S. E., Springston, S. R., Chaigneau, A., Toniazzo, T., Minnis, P., Palikonda, R., Abel, S. J., Brown, W. O. J., Williams, S., Fochesatto, J., Brioude, J., and Bower, K. N.: The VAMOS Ocean-Cloud-Atmosphere-Land Study Regional Experiment (VOCALS-REx): goals, platforms, and field operations, Atmos. Chem. Phys., 11, 627–654, doi:10.5194/acp-11-627-2011, 2011.